Supporting Information

Solution-Dispersible Metal Nanorings with Deliberately Controllable Compositions and Architectural Parameters for Tunable Plasmonic Response

Tuncay Ozel, [†,¥] *Michael J. Ashley,* [‡,¥] *Gilles R. Bourret,* [ɣ] *Michael B. Ross,* [ɣ] *George C. Schatz,** [ɣ] *and Chad A. Mirkin** [†,‡,ɣ]

[†]*Department of Materials Science and Engineering,* [‡]*Department of Chemical and Biological Engineering,* [ɣ]*Department of Chemistry, and International Institute for Nanotechnology, Northwestern University, Evanston, Illinois 60208, United States*

[¥]These authors contributed equally

*E-mail: chadnano@northwestern.edu, schatz@chem.northwestern.edu

Materials and Methods

Materials and Chemicals: All chemicals and solutions were used without further processing. Commercially available plating solutions (Cyless for Ag, Orotemp 24 Rack for Au, Pallaspeed VHS for Pd, and nickel sulfamate for Ni) were purchased from Technic Inc., USA. Aniline (≥99.5%), 70% aqueous perchloric acid (99.999%), 70% aqueous nitric acid, 49-51% aqueous phosphoric acid, ammonium hexachloroplatinate (99.999%), sodium phosphate dibasic (99%), sodium hydroxide (≥98%), iron (III)

chloride hexahydrate (97%), 28-30% aqueous ammonium hydroxide, and sodium citrate (≥99%) were purchased from Sigma-Aldrich, USA. 30% aqueous H_2O_2 was purchased from VWR, USA. AAO membranes with 35, 55 and 100 nm nominal pore diameters were purchased from Synkera Technologies Inc., USA. AAO membranes with 270 nm nominal pore diameters were purchased from Whatman Inc., USA.

Instruments: High-angle annular dark-field imaging z-contrast (ZC mode) scanning transmission electron microscope (STEM) images and energy dispersive X-ray spectroscopy (EDX) maps were acquired using a Hitachi HD-2300 STEM. SEM images were collected on a Hitachi SU-8030 SEM. Electrochemical deposition of metals and inorganic semiconductors were done using a BASi EC epsilon potentiostat (Bioanalytical Systems, Inc., USA). A Kurt J. Lesker PVD 75 e-beam evaporator was used to evaporate Ag films onto AAO templates. All UV-Vis-NIR data were obtained using a Cary 5000 spectrometer.

Electrochemical Deposition Parameters: Depositions were done at constant potentials using aqueous electroplating solutions as detailed below.

- **Au** was deposited at -950 mV (270 and 100 nm template) and -1100 mV (55 and 35 nm template) using Orotemp 24 Rack solution.
- **Ag** was deposited at -910 mV using Cyless solution.
- **Pd** was deposited at -900 mV using Pallaspeed VHS solution.
- **Ni** was deposited at -930 mV (270 and 100 nm template) and -1100 mV (55 and 35 nm template) using nickel sulfamate solution.
- **Pt** was deposited at -500 mV using a homemade aqueous Pt solution (15 mM $(NH_4)_2PtCl_6$ and 200 mM Na_2HPO_4).

- **Polyaniline (PANI):** PANI was deposited at +1000 mV, using a homemade solution containing 680 μL of aniline dissolved in 15 mL of a 0.1 M $HClO_4$ aqueous solution.

Details of the Nanoring Synthesis

Templated nanoring synthesis began with porous anodized aluminum oxide (AAO) membranes coated with a 350 nm thick Ag layer that acts as the working electrode during electrodeposition. For the 35 and 55 nm template syntheses, AAO is first exposed to 0.5 M NaOH for 2 minutes. This step (termed "pore refinement," see Figure S2 for 35 nm templates pore-refined up to 9 minutes) serves to modestly enlarge the pore size of the smaller AAO templates to guarantee that the subsequent steps can be reproducibly performed. We have also observed that pore refinement improves the uniformity of AAO pores (refer to Figure S2). This step is not performed when using 100 nm templates to allow for for diameter tuning in the later steps. Electrochemical deposition was carried out using a three-electrode setup, as described elsewhere in detail.[1-4] First, Ag and Ni were successively deposited within the AAO membrane. Next, a polyaniline (PANI) core was deposited and samples were dried under light vacuum for 30 minutes to create space between the polymer segments and the walls of the AAO pores. As the Ni base was more conductive than the PANI core, subsequent electrodeposition led to our materials of interest filling this shell space from the bottom up rather than forming on top of PANI. However, before shell deposition, both the final outer and inner diameters of the nanorings were determined. A pore-widening step was first conducted in which the AAO membrane was exposed to 0.5 M NaOH for 3 to 18 minutes. In this step, the NaOH solution traveled down into the AAO pores and slowly

dissolved the template from the inside out. This created more space between PANI and the pore walls, ensuring that fully-formed ring structures were later synthesized (a minimum of 3 minutes was required for this to be reliable), and allowing for outer diameter tunability. Pore-widening for beyond 18 minutes, however, resulted in partial merging of some pores and inconsistent shell deposition.

Particularly for 35 nm AAO templates, the initial pore refinement step was critical to ensure that every step until this point occurred with complete reproducibility. Without it, PANI was not guaranteed to contract enough to allow sufficient space for NaOH to widen the pores such that full rings were consistently generated.

In order to achieve inner diameter control, the template was first pore-widened (18 minutes for the 100 nm template sample with inner diameter reduction, and 10 minutes for the 35 nm template sample; inner diameter reduction was not performed on the 55 nm template sample) and then exposed to a 70% ethanol solution in water for 30 minutes. Within each pore, ethanol slowly dissolved PANI from all sides such that the core material diminished in size and the resulting rings had a reduced inner diameter. The previous pore-widening step was necessary as it increased the amount of ethanol that PANI was exposed to on its sides relative to its top, maximizing inner diameter reduction. The use of a 70% ethanol solution for 30 minutes was found to result in the smallest average inner diameter for the rings without the resulting solution being composed of a mixture of rings and disks. When PANI was exposed to ethanol either in a more concentrated solution or for longer times, the (several micron long) polymer segment dissolved too much from the top, such that the subsequently electrodeposited material reached beyond it in some of the pores and formed a disk. It was also observed that the

polymer thinning slows with time, such that thinning with 70% ethanol for 30 minutes reduces polymer diameter nearly as much as thinning with 80% ethanol renewed with 90% ethanol for 30 minutes each. The latter case, however, leads to a solution with both rings and disks.

Additionally, ethanol solutions of varied concentration for varied time periods can be used to achieve nanorings with inner diameters intermediate to those reported in the main text. This possibility is depicted in Figure S3, which shows the polymer segment encased in Ni after different ethanol exposures. In these experiments, the Ni diameter represents the hypothetical outer diameter of a nanoring (if a target material had been deposited), and the polymer diameter represents the hypothetical inner diameter of a nanoring. It is clear that by varying ethanol concentration and exposure time, a range of inner diameters can be obtained.

After pore-widening and (optional) polymer thinning with ethanol, sequential deposition of a sacrificial shell segment and a target material shell segment (the desired nanoring) finalize the templated portion of the synthesis. The amount of charge passed during electrodeposition controlled the shell segment length, and thus the final nanoring length. Au and Pt nanorings were synthesized by depositing a Ni sacrificial segment followed by Au/Pt. Ag nanorings were synthesized by depositing alternating Ni-Ag-Ni shell segments. Pd and Ni nanorings were synthesized by depositing a Ag sacrificial shell segment followed by Pd/Ni. For the multi-component (Au-Ni-Pt) tube, a sacrificial Ni shell segment was deposited onto a short Ni base before Au-Ni-Pt. For Au, Pt, Pd, Ag, and multi-component nanoring syntheses, the Ag backing layer was dissolved using a mixture of 30% aqueous H_2O_2 (Macron, Inc.) and 28-30% aqueous NH_4OH (Sigma-

Aldrich) (1:1 v:v). For Ni nanoring synthesis, the Ag backing layer and Ni base segment were removed by mechanical polishing with HNO_3. For the multi-component synthesis, the Ni sacrificial segments were removed by exposing the bottom of the template (the side from which Ag was just removed) to 3% aqueous $FeCl_3$ for 20 minutes to selectively remove the Ni base and first shell segment, while leaving the target Ni intact. After immersing in water for at least 5 minutes in all cases, AAO membranes were placed in acetone for at least 2 hours in order to fully dissolve PANI. Templates were then dissolved in 0.5 M NaOH. The remaining structures were then centrifuged at 9000 rpm for 3 minutes, and sacrificial materials were removed with 3% $FeCl_3$ in water for 20 minutes for Au and Pt nanorings, 15% H_3PO_4 in water for 15 minutes for Ag nanorings, and the H_2O_2/NH_4OH mixture mentioned above for Pd and Ni nanorings (this step is not necessary for the multi-component sample). Nanorings were centrifuged at 10,500 rpm for 6 minutes 3 times and resuspended in water with 0.1% sodium citrate by weight. For all materials other than Au, samples were always pore widened for 18 minutes. Polymer thinning in 70% ethanol was performed for Ag (10 minutes).

TEM images were also obtained of structures before final etching of the sacrificial segments, as pictured below in Figure S4. Nanoring lengths were most easily measured this way.

Alternatively, if top view SEM images of nanorings (as pictured in Figures 1 and 2 of the main text) were desired, the order of selective etching/dissolving was changed. After nanoring deposition, PANI was dissolved in acetone for 2 hours. Then, templates were placed on carbon tape and immersed in 0.5 M NaOH overnight to ensure full dissolution of AAO. After washing with water, an array of nanorod/nanotube structures

remained with the target ring material visible on top. Measurements of ring outer and inner diameters were performed on top view SEM images of these structures using Adobe Photoshop (described below). Rings can be dispersed into solution in this way by exposing the templates to the sacrificial segment etchant.

Photoshop Characterization: Outer and inner diameters of the Au rings were measured using Adobe Photoshop CS5. Top view SEM images were taken of rings on top of the sacrificial Ni and Ag segments, with PANI and the AAO template having been dissolved (See Figure 1 in the main text). Traces were drawn around the outer and inner surfaces of each ring (sample size = 50), yielding measurements of the area and perimeter of both in nm^2 and nm, respectively. From these measurements, both the outer and inner diameters of rings could be calculated. By using this measurement technique (rather than a linear measurement), we eliminated the bias of choosing where to measure these lengths in the cases of imperfect rings. Table S1 below summarizes the statistics of Au ring architectural parameters. Circularity, as reported in Figure S2, is similarly calculated by Photoshop. It is defined as the ratio of the radius of a circle inscribed in a given shape to that of a circle circumscribed about the same shape such that a perfect circle has a circularity of 1. Here we use it to analyze the shape of AAO pores.

Extinction Spectrum Simulations

The extinction spectra of nanorings were simulated using the discrete dipole approximation (DDA) using an implementation developed by Draine and Flatau.[5] In this, an object of arbitrary shape is described as a simple cubic array of dipoles. Maxwell's Equations are then solved numerically such that the fields are fully retarded. For the Au

nanoparticles studied here, the dielectric constants from Johnson and Christy were used and a surface scattering correction was included to remove unphysical LSPR lineshapes. All structures used a dipole spacing of 1nm/dipole except for the largest ring (Figure S7d), which was simulated with a spacing of 4nm/dipole to allow convergence. Each simulation was performed for three orientations of the ring (in-plane, out-of-plane, and face incident). These were averaged to reproduce the orientation averaging observed in solution.

Supplementary Figures and Table:

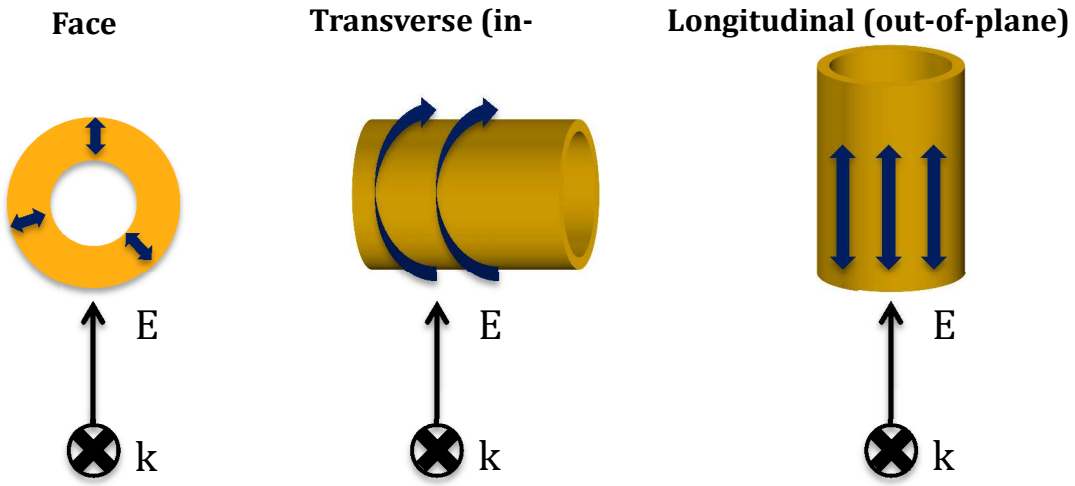

Figure S1. The three characteristic surface plasmon resonance modes of nanorings.

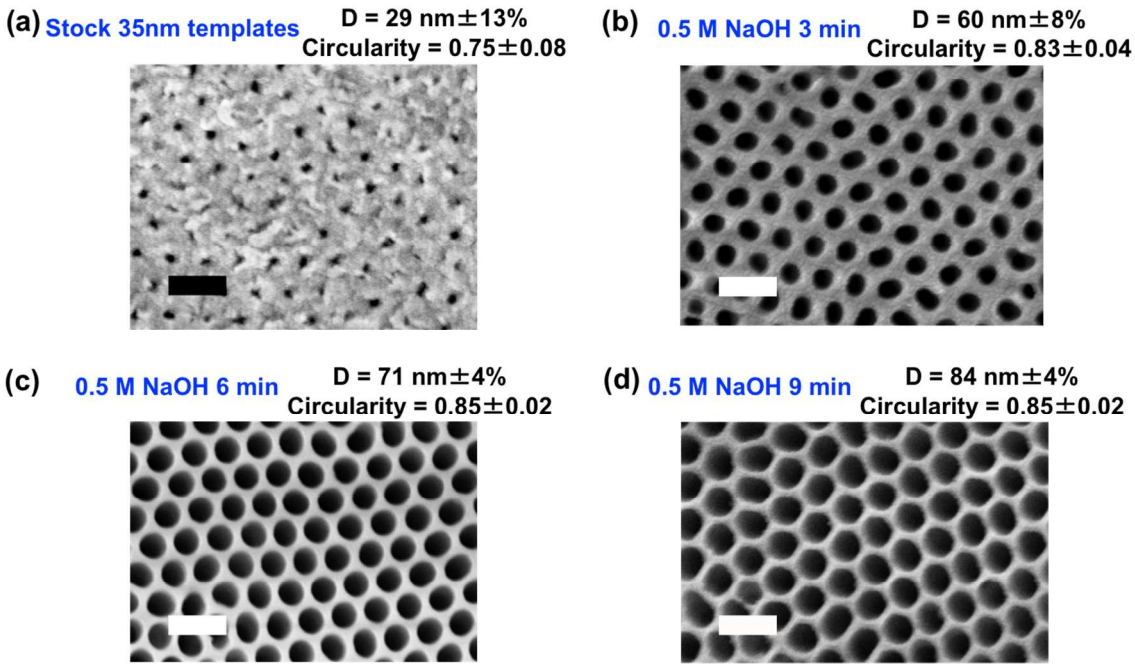

Figure S2. Analysis of a 35 nm template pore refined for (a) 0, (b) 3, (c) 6, and (d) 9 minutes by exposure to 0.5 M NaOH. Scale bars are 100 nm.

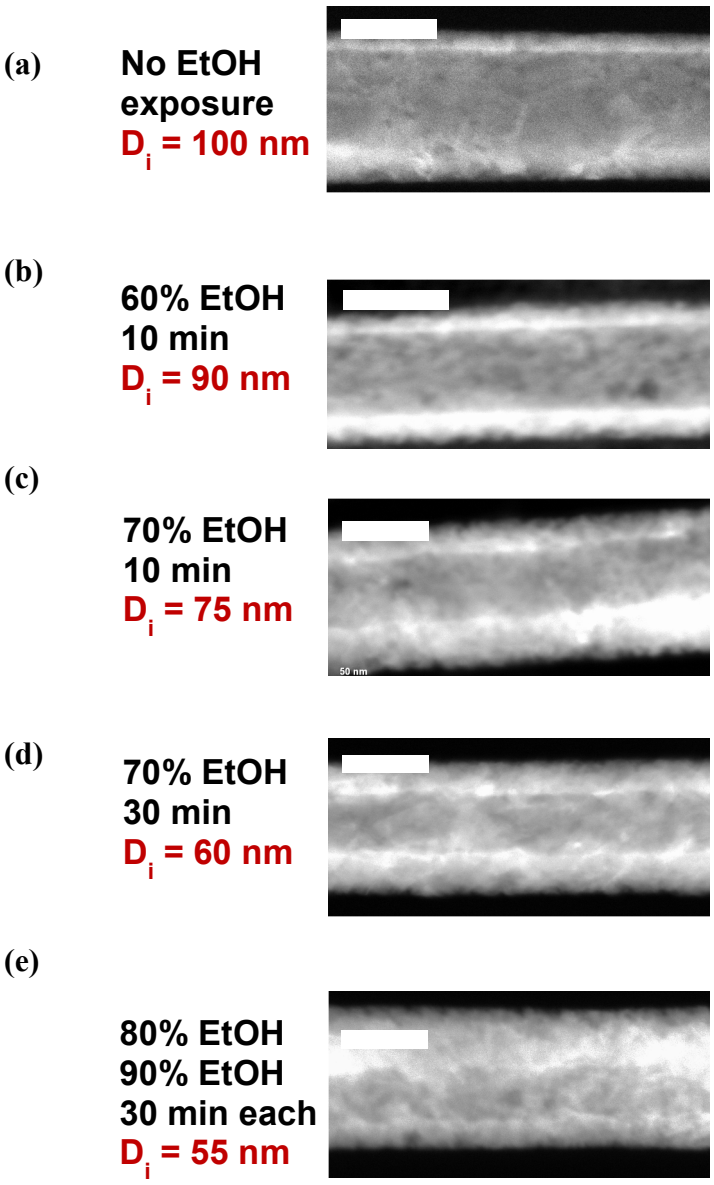

Figure S3. STEM images of PANI (dark contrast) encased in Ni (light contrast), showing the reduction in PANI diameter (D_i) with increasing ethanol concentrations and times. Pictured are samples treated with: (a) no ethanol exposure, (b) 60% ethanol for 10 minutes, (c) 70% ethanol for 10 minutes, (d) 70% ethanol for 30 minutes, and (e) 80% ethanol for 30 minutes renewed with 90% ethanol for an additional 30 minutes. Ni diameters are effectively constant at around 160 nm. Only a slight decrease in diameter is observed between samples with 70% EtOH treatment for 30 minutes and 80% EtOH renewed with 90% EtOH for 30 minutes each. The former yields a pure nanoring solution whereas the latter yields a mixture of rings and disks. Scale bars are 100 nm.

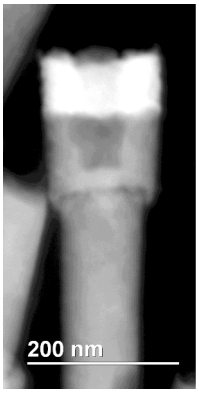

Figure S4. STEM image of a Au nanoring with sacrificial Ni shell segment and Ni base. The effect of pore-widening is evident from the difference in diameter of the Ni rod base and the shell segments.

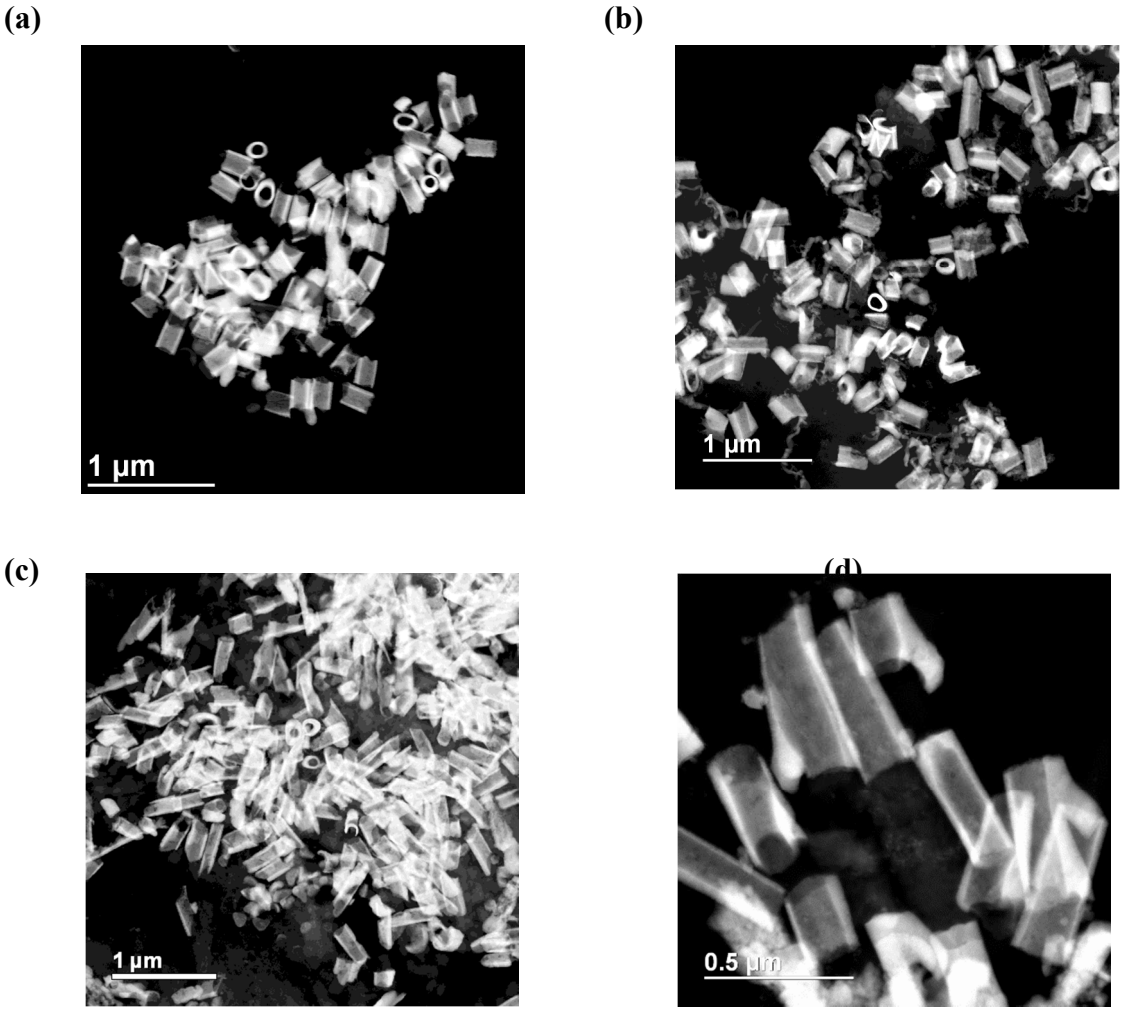

Figure S5. STEM images of nanorings composed of (a) Pt, (b) Ag, (c) Pd, and (d) Ni. An image for Au nanorings is provided in Figure 1 of the main text. It is worth noting that most of the nanorings presented in this figure were imaged in their side-view orientation since nanorings with aspect ratios greater than 1 (height:diameter) tend to land on their longer edge as opposed to their shorter edge.

(a)

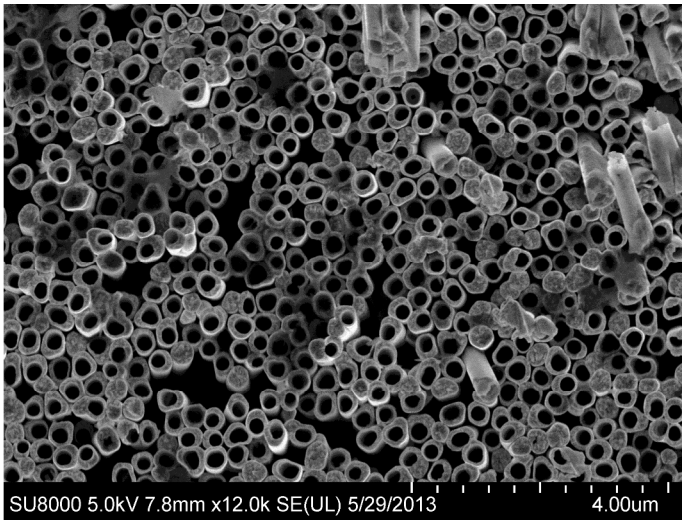

(b)

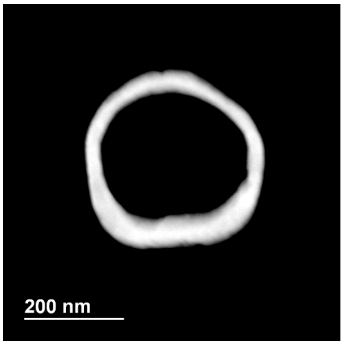

Figure S6. Largest Au nanorings synthesized in 270 nm pore diameter template. **(**a) Top view SEM image used to measure average inner and outer diameters. (b) STEM image of a single nanoring in solution.

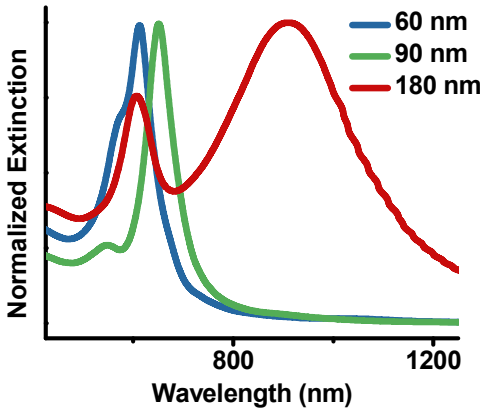

Figure S7. Calculated extinction spectra (orientation-averaged) of Au nanorings with increasing outer diameters. The spectra for the 60 and 90 nm outer diameter samples match the experimental data in Figure 3 of the main text quite closely.

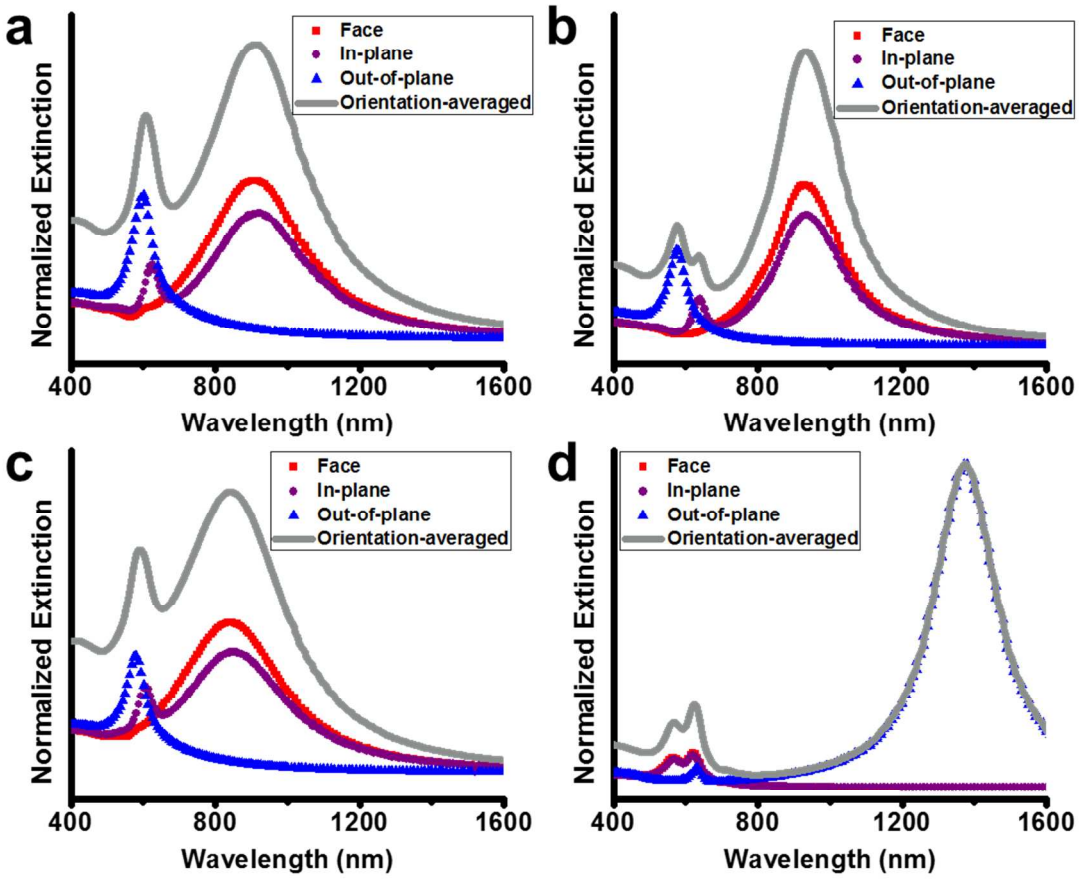

Figure S8. Calculated extinction spectra (detailed to illustrate the face, in-plane, and out-of-plane plasmonic modes individually and orientation-averaged) of Au nanorings referred to as (a) 18 min widened, (b) 3 min widened, (c) 18 min widened+thinned, (d) 18

min widened (tall) in the main text Figure 3. Note that we are unable to synthesize or simulate a nanoring sample that separates all three LSPRs, as the face and in-plane resonances are nearly always positioned at the same wavelength.

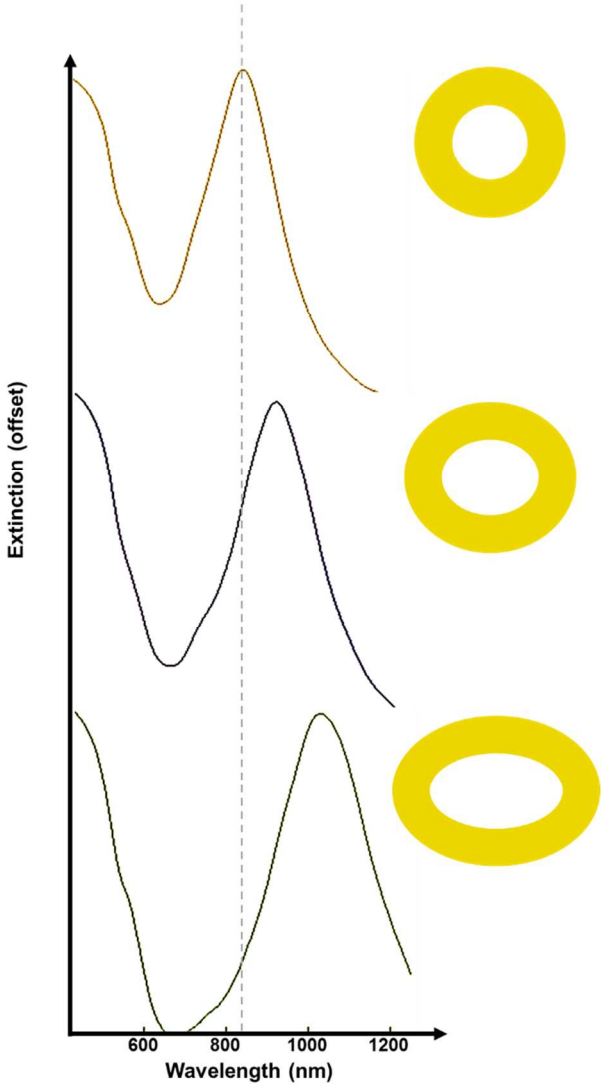

Figure S9. Calculated extinction spectra (in-plane plasmon resonances) of elliptical Au nanostructures. For Au nanorings of 80 nm fixed height, inner and outer dimensions of the nanorings (in the x-y plane) are modified to resemble elliptical nanostructures similar to those observed in the top-view SEM images presented in Figure 2 of the main text. Nanoring dimensions in the y-axis were kept fixed (80 and 160 nm for the inner and the outer diameters, respectively) whereas the inner and the outer dimensions defined in the x-axis are (top) 80 and 160 nm, (middle) 102 and 182 nm, (bottom) 140 and 220 nm. The spectra are offset for clarity. The experimental extinction spectra shown in Figures 3 and 4 are red-shifted from the simulations for all 100 nm template samples. The simulations shown here suggest that dispersity in nanoring shape (circular vs. elliptical) could

account for some of this discrepancy between simulated and experimental extinction spectra. We also observe a slight broadening of the extinction peaks with greater elliptical shape.

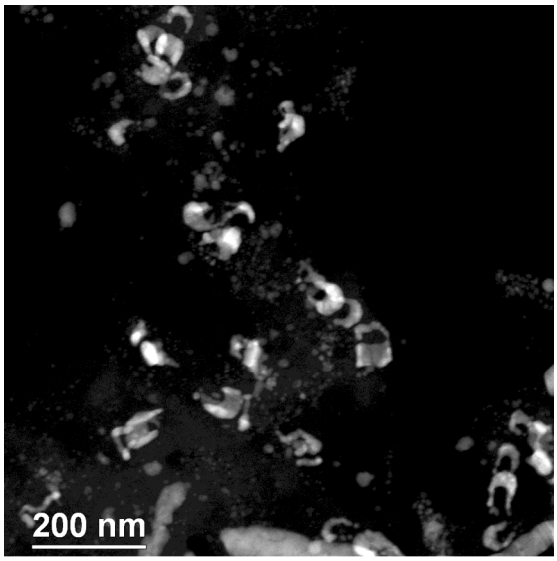

Figure S10. STEM image of broken and malformed rings resulting from insufficiently long Au ring segments in a 35 nm pore diameter template sample.

Table S1. Summary of Au ring dimensions demonstrating both coarse and fine tuning of length parameters. Sample size = 50 for all cases. Reported error measurements represent one standard deviation. For each sample, the critical varied parameter is displayed in red font.

Nominal pore diameter (nm)	Pore refinement in 0.5 M NaOH	Pore widening in 0.5 M NaOH	Polymer thinning	Outer diameter (nm)	Inner diameter (nm)	Height (nm)	Aspect Ratio (outer diameter/height)	Main Text Ref.
100 **(base case)**	None	18 min	None	178.9±17.2	95.0±11.5	82.9±7.1	0.46±0.06	Figs. 3, 4
100	None	3 min	None	156.1±16.0	96.3±11.7	60.7±8.5	0.39±0.07	Fig. 4a
100	None	18 min	None	177.5±17.1	94.6±10.2	318.9±28.1 (5x charge as base-case sample)	1.80±0.23	Fig. 4c
100	None	18 min	30 min 70% EtOH	177.4±15.9	63.9±11.0	73.6±7.0	0.41±0.05	Fig. 4b
35	2 min	10 min	30 min 70% EtOH	63.2±5.1	25.6±3.3	47.2±4.3	0.75±0.09	Fig. 3
55	2 min	15 min	None	95.1±9.6	36.7±6.0	41.5±6.5	0.44±0.08	Fig. 3
270	None	20 min	None	395.8±29.5	233.4±19.7	N/A	N/A	-

References

1. Osberg, K. D.; Schmucker, A. L.; Senesi, A. J.; Mirkin, C. A. *Nano Lett.* **2011,** *11*, 820-824.
2. Banholzer, M. J.; Qin, L.; Millstone, J. E.; Osberg, K. D.; Mirkin, C. A. *Nat. Prot.* **2009,** *4*, 838-848.
3. Qin, L.; Park, S.; Huang, L.; Mirkin, C. A. *Science* **2005,** *309*, 113-115.
4. Ozel, T.; Bourret, G. R.; Mirkin, C. A. *Nat. Nanotechnol.* **2015,** *10*, 319-324.
5. Draine, B. T.; Flatau, P. J. *J. Opt. Soc. Am. A* **1994,** *11*, 1491-1499.